J. Fluid Mech. (2009), *vol.* 621, *pp.* 259–288. © 2009 Cambridge University Press
doi:10.1017/S0022112008004874 Printed in the United Kingdom

High-Reynolds-number turbulent boundary layer friction drag reduction from wall-injected polymer solutions

E. S. WINKEL[1], G. F. OWEIS[2], S. A., VANAPALLI[3], D. R. DOWLING[1], M. PERLIN[1], M. J. SOLOMON[1] AND S. L. CECCIO[1]†

[1]University of Michigan, Ann Arbor, MI, USA

[2]American University of Beirut, Lebanon

[3]Texas Tech University, Lubbock, TX, USA

(Received 29 October 2007 and in revised form 17 October 2008)

A set of controlled high-Reynolds-number experiments has been conducted at the William B. Morgan Large Cavitation Channel (LCC) in Memphis, Tennessee to investigate the friction drag reduction achieved by injecting aqueous poly(ethylene oxide) (PEO) solutions at three different mean molecular weights into the near-zero-pressure-gradient turbulent boundary layer that forms on a smooth flat test surface having a length of nearly 11 m. The test model spanned the 3.05 m width of the LCC test section and had an overall length of 12.9 m. Skin-friction drag was measured with six floating-plate force balances at downstream-distance-based Reynolds numbers as high as 220 million and free stream speeds up to 20 m s^{-1}. For a given polymer type, the level of drag reduction was measured for a range of free stream speeds, polymer injection rates and concentrations of the injected solution. Polymer concentration fields in the near-wall region ($0 < y^+ < \sim 10^3$) were examined at three locations downstream of the injector using near-wall planar laser-induced-fluorescence imaging. The development and extent of drag reduction and polymer mixing are compared to previously reported results using the traditional K-factor scaling. Unlike smaller scale and lower speed experiments, speed dependence is observed in the K-scaled results for the higher molecular weight polymers and it is postulated that this dependence is caused by molecular aggregation and/or flow-induced polymer degradation (chain scission). The evolution of near-wall polymer concentration is divided into three regimes: (i) the development region near the injector where drag reduction increases with downstream distance and the polymer is highly inhomogeneous forming filaments near the wall, (ii) the transitional mixing region where drag reduction starts to decrease as the polymer mixes across the boundary layer and where filaments are less pronounced and (iii) the final region where the polymer mixing and dilution is set by the rate of boundary layer growth. Unlike pipe-flow friction-drag reduction, the asymptotic maximum drag reduction (MDR) either was not reached or did not persist in these experiments. Instead, the nearest approach to MDR was transitory and occurred between the development and transitional regions. The length of the development region was observed to increase monotonically with increasing polymer molecular weight, injection rate, concentration and decreasing free stream speed. And finally, the near-wall polymer concentrationis correlated to the measured drag reduction for the

† Email address for correspondence: ceccio@umich.edu

https://doi.org/10.1017/S0022112008004874 Published online by Cambridge University Press

three polymer molecular weights in the form of a proposed empirical drag-reduction curve.

1. Introduction

Reduction of turbulent boundary layer skin friction in external flows is an enduring priority for performance improvement in marine transportation systems. Researchers have known for more than 50 years that the presence of high-molecular-weight polymers in the near-wall region of a turbulent boundary layer (TBL) can reduce friction drag by as much as 70 % compared to a corresponding flow of pure water, even when the polymer concentration is only a few tens of weight parts per million (w.p.p.m.). The mechanisms of polymer drag reduction (PDR) have been under investigation for several decades, and an overall picture of the interaction of the long-chain polymers with turbulence has emerged through analytical, experimental and numerical studies. Dubief *et al.* (2004) discuss in detail how the stretching and recoiling of polymer molecules in the near-wall flow can modify the usual self-sustained near-wall turbulence regeneration cycle involving buffer-layer vortices and viscous sub-layer streaks (Jimenez & Pinelli 1999). Here, the polymer extracts energy from the buffer-layer vortices and releases it in the near-wall streaks leading to enhanced streamwise velocity fluctuations, reduced wall-normal velocity fluctuations and increased streamwise vortex spacing in the near-wall region. The near-wall shear stress balance is then a combination of viscous, Reynolds and (non-trivial) polymer stresses. Finally, the state of maximum drag reduction (MDR) is achieved when there is sufficient polymer in the near-wall region to produce a new self-sustained turbulence regeneration cycle. Once MDR is achieved, further increases in polymer concentration do not reduce friction drag. Instead, higher polymer concentrations may increase friction drag via increased shear viscosity. The detailed interaction of the polymer with turbulent flow is still the object of study, but this phenomenological description is consistent with experimental observations of drag reduction, including the recent work of Warholic, Massah & Hanratty (1999), Ptasinski *et al.* (2003) and White, Somandepalli & Mungal (2004).

Polymer additives are used commercially to reduce friction in internal flows (Sellin 1982) where the polymer is uniformly mixed throughout the fluid and drag reduction is constant along the length of the pipe (in the absence of degradation). However, in external-flow applications, mixing and dilution of the polymer with the free stream – and possibly polymer degradation – generally cause PDR to decay with increasing downstream distance. Prior flat-plate TBL PDR studies commonly use aqueous polymer solutions of poly(ethylene oxide) (PEO) and polyacrylamide and have reached downstream-distance-based Reynolds numbers up to $Re_x = 45$ million (Vdovin & Smol'yakov 1981) and free stream speeds up to $16.8\,\mathrm{m\,s^{-1}}$ (Petrie, Brungart & Fontaine 1996). In such experiments, the polymer solution was injected into a TBL via a spanwise slot on the wall on which the boundary layer forms. The experimental results reported here are for higher Reynolds number, up to $Re_x = 220$ million, but utilize aqueous PEO solutions and simple spanwise slot injection, as in prior experiments.

Transport and dilution of the injected polymer solution in a TBL have been measured experimentally by adding a dye tracer to the injected polymer and extracting samples of near-wall fluid (Fruman & Tulin 1976; Vdovin & Smol'yakov 1978, 1981)

https://doi.org/10.1017/S0022112008004874 Published online by Cambridge University Press

or by laser-induced fluorescence (LIF) (Fontaine, Petrie & Brungart 1992). During PDR, the turbulent transport of near-wall polymer in a TBL (Poreh & Hsu 1972) is reduced relative to that of a passive scalar (Poreh & Cermak 1964), consistent with the observed reduction in skin friction. In the experiments reported here, unique co-located skin-friction and polymer-concentration-imaging measurements were made that allow the morphology of the near-wall polymer to be linked to the state of PDR in the boundary layer.

Degradation (chain-scission) of long-chain polymer molecules in the turbulent flow is also a concern for effective PDR. Prior investigations of polymer degradation have been conducted primarily in pipe flows and rotational Taylor–Couette flow devices. Currently, no direct measurements of polymer degradation in TBL flows have been reported. In pipe flows, Horn & Merrill (1984) have shown that the polymer chains break near the mid-point, where stresses on the polymer chain are highest. Vanapalli, Islam & Solomon (2005) and Vanapalli, Ceccio & Solomon (2006) provide scission relationships for PEO that indicate that chain-scission occurs in PEO solutions at shear rates lower than those of previous and the present TBL PDR studies. Thus, polymer degradation may play a role in the current experiments especially because of their relatively long downstream extent.

Application of PDR to large-scale external flows necessitates an understanding of how the injected polymer mixes (and possibly degrades) as it is transported downstream. Moreover, for scaling purposes, it is useful to understand how experimental results at moderate Reynolds numbers compare to similar results at higher speeds and larger length scales. In particular, it is important to determine: (i) the downstream evolution of near-wall ($y^+ < \sim 10^3$) polymer concentration since there is no PDR without near-wall polymer; (ii) the downstream persistence of PDR given the aforementioned effects of mixing, dilution and degradation; and (iii) the influence of the polymer's molecular and rheological properties on the resulting near-wall concentration and PDR. The experimental study reported here, in conjunction with prior PDR studies, addresses these three issues. Measured relationships between polymer mean molecular weight, injection concentration, injection flux, free stream speed and the resulting drag reduction and turbulent polymer diffusion are reported. The traditional K-parameter scaling for percentage drag reduction ($\%DR$) and near-wall concentration is discussed, and results from the present experiments are compared with those of prior smaller scale studies. The relationship between near-wall polymer concentration and the drag reduction is also examined and presented in the form of an empirical scaling law. The possibility of flow-induced polymer degradation and the potential role of polymer aggregation are discussed as well.

The remaining paper is divided into seven sections. The next section presents the experimental techniques. The third section concisely describes the relevant baseline flow results. Polymer rheology, polymer drag reduction and near-wall polymer concentration measurements are presented in the fourth, fifth and sixth sections, respectively. Observed and expected levels of PDR are compared in the seventh section. The final section provides a summary of this effort and the conclusions drawn from it.

2. Experimental methods

2.1. *Test facility and model*

Experiments were conducted in the William B. Morgan Large Cavitation Channel (LCC), the world's largest low-turbulence (free stream turbulence <0.5 %),

https://doi.org/10.1017/S0022112008004874 Published online by Cambridge University Press

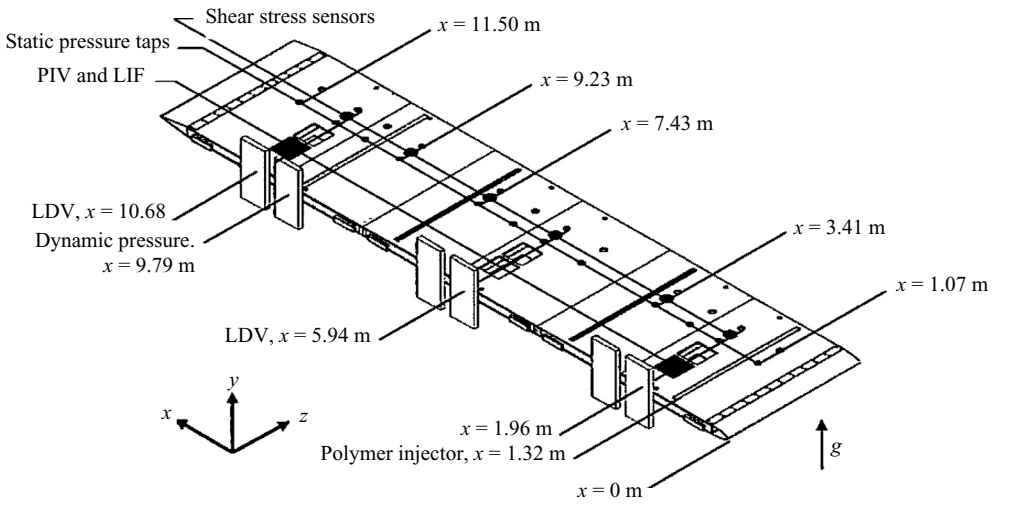


FIGURE 1. Schematic drawing of the large flat-plate test model with injection and measurement locations. The model was inverted in the LCC test section; so the underside of the test model is shown here. The x-axis is parallel to the flow direction.

re-circulating water tunnel (Etter *et al.* 2005). The dimensions of the test section are 16 m (length) and 3.05 m × 3.05 m (width and height). The test model was a 12.9 m long, 3.05 m wide and 0.18 m thick rigid flat plate, spanning the entire width of the LCC test section. The model and its installation in the LCC are described in Sanders *et al.* (2006), so only a brief summary is provided here. The model's leading edge was a 4:1 ellipse and its trailing edge was a 15° full-angle truncated wedge. The model was positioned near the vertical centreline of the LCC test section with the test surface facing downward. The boundary layer was tripped via distributed roughness applied to the first 0.30 m of the model. Otherwise, the test surface was polished 304 stainless steel with a root-mean-square surface roughness of $k < 0.4$ μm, small enough for the surface to be considered hydrodynamically smooth at all test speeds. The test surface was instrumented as shown in figure 1.

2.2. *Polymer mixing and injection*

The polymers used in this experiment were poly(ethylene oxide) (PEO or POLYOX) water-soluble powdered resins manufactured by Dow Chemical Company: WSR-N60K, WSR-301 and WSR-308. These polymers have manufacturer-specified mean molecular weights M_w of approximately 2, 4 and 8 million, respectively. In the case of WSR-N60K, the manufacturer's M_w was checked by means of gel permeation chromatography (GPC) with light scattering detection (Vanapalli *et al.* 2005). The WSR-N60K measured M_w and polydispersity index were 2.3×10^6 g mol^{-1} and 2.44, respectively. Attempts to assess the M_w of WSR-301 and WSR-308 by the same technique failed, likely due to molecular aggregation (Vanapalli 2007).

For all three powdered resins, aqueous polymer solutions were prepared by sifting the powder into a jet of water that filled the main solution-preparation reservoir. The water was filtered prior to mixing with an activated carbon filter (Model RT-2260-4, Aquapure Technologies) to remove chlorine as chlorine is potential for chemical degradation of PEO (Petrie *et al.* 2003). After this initial wetting, the polymer solution was stirred in the 4.55 m^3 reservoir with a 4-blade 0.75 m diameter impeller at 30 r.p.m. until homogeneous, this stirring process typically taking 1–3 days.

https://doi.org/10.1017/S0022112008004874 Published online by Cambridge University Press

In addition, two small trolling motors were used near the reservoir surface to break-up and homogenize near-surface polymer agglomerations. The effectiveness and repeatability of the mixing process and the stability of the polymer solutions were verified using a 4.57 mm diameter pipe-flow pressure-drop apparatus to characterize the drag-reducing behaviour of the solutions. Test results showed that the mixing process was repeatable and that the solution's drag-reducing capacity was stable over a period of 115 h.

After hydration and mixing, the polymer was transferred to a smaller 1.140 m^3 tank that fed a low-shear-rate stainless-steel progressive-cavity pump (Moyno, model 2E012G1SSQAAA-158587). This pump delivered the polymer to an injection manifold inside the test model having 40 evenly spaced ports along the injector span. Inside this manifold, three layers of perforated plates and brass screens generated a pressure drop to ensure spanwise uniformity of the injection flow. The actual injector was a simple tapered slot with an outlet gap of 1 mm, oriented with mean angle of 25° with respect to the test surface. This injector is similar to one used in an optimization study by Walker, Tiederman & Luchik (1986) and its design is consistent with injectors in prior PDR experiments.

As mixing, pumping and flow upstream of the injector outlet may potentially degrade the polymer prior to injection, the polymer delivery system was designed to minimize the potential for degradation based on the PEO degradation results of Vanapalli *et al.* (2005) (see also §4). In addition, polymer solution samples were collected after passage through the delivery system. When characterized using the 4.57 mm diameter pipe-flow apparatus, the collected-sample pressure-drop results matched those of polymer solution drawn directly from the reservoir above the injection pump.

2.3. *Experimental parameters and procedures*

The experimental conditions involved three free stream velocities ($U = 6.65$, 13.2 and 19.9 m s^{-1}), three nominal polymer molecular weights ($M_w = 2$, 4 and 8 million), three injection concentrations ($C_i = 1000$, 2000 and 4000 w.p.p.m. of polymer) and three volumetric injection rates ($Q_i = 0.14$, 0.28 and 0.71 l $s^{-1}m^{-1}$). When normalized with a standard volume flux per unit span, $Q_s = 67.3\,\nu$ (Wu & Tulin 1972), where ν is the kinematic viscosity of the free stream liquid, and these injection rates correspond to $Q_i/Q_s = 2$, 4 and 10.

Percentage drag reduction was computed directly from steady-state shear stress measurements with ($\tau_{w,i}$) and without (τ_w) polymer injection:

$$\%DR = \frac{\tau_w - \tau_{w,i}}{\tau_w} \times 100. \tag{2.1}$$

Once a steady-state skin friction was observed after the start of polymer injection, polymer concentration measurements were initiated. Data acquisition was usually complete in one to several minutes, at which point the polymer injection pump was stopped. To reduce bias error in the shear stress measurements, the buildup of active polymer in the free stream flow was monitored carefully. When the no-injection shear stress τ_w was reduced by more than 2 % (approximately half the random shear stress measurement error), a controlled amount of chlorine was added to the tunnel water to chemically degrade the background polymer. The free chlorine is consumed as it reacts with the polymer, so the amount of chlorine added between runs was adjusted to leave only trace amounts, much less than 1 p.p.m. In addition, the background chlorine level was continually monitored to ensure that an excess of chlorine did

https://doi.org/10.1017/S0022112008004874 Published online by Cambridge University Press

not occur. As a backup measurement, samples of the tunnel water were removed periodically and tested in the aforementioned pipe-flow apparatus to ensure that mildly contaminated tunnel water did not bias the drag-reduction results. In addition, throughout the course of these multi-month tests, the entire water volume of LCC ($5300\,\mathrm{m}^3$) was flushed and refilled weekly.

2.4. *Skin-friction drag balances*

Direct skin-friction measurements were made at six streamwise locations using floating-plate strain-gauge type friction drag sensors, as shown in figure 1. The floating-plate elements were polished 17-4PH stainless steel, 15.2 cm in diameter and 0.79 cm thick. Each floating-plate was attached to the load-sensing element, a beryllium copper flexure instrumented with a full Wheatstone bridge of semiconductor strain gages. The plate and flexure were mounted within a bowl-shaped housing so that the plate and housing edge were flushed with the model's test surface. The gap between the floating-plate and housing was measured with feeler gauges to be $60 \pm 20\,\mu\mathrm{m}$. The strain gages were excited at 7 VDC using signal-conditioning amplifiers (Model # 2310, Vishay Measurements Group). The sensor outputs were amplified 500-fold and low-pass filtered at 10 Hz with the same Vishay units. The amplified and filtered signals were recorded simultaneously at 50 Hz.

The skin-friction sensors were calibrated from 0 to 10 N ($\sim$2 lb) with increasing and decreasing loads using a second load cell (Model LCEB-5, Omega Engineering) mounted horizontally downstream of the friction balance. A cable was tied between a suction cup on the floating-plate and the second load cell that was mounted on a linear traverse used to increase or decrease the cable tension. The error associated with the sensor slope was taken to be twice the standard deviation of multiple calibration slopes (typically five or more) and varied between 0.8 % and 2.9 %. The overall uncertainty in any skin-friction measurement was typically less than ± 5 %.

2.5. *Polymer concentration measurements*

Planar laser-induced flourescence (PLIF) was used to measure the polymer concentration in the near-wall region of the TBL. Measurements were made at three streamwise locations $X - X_i = 0.64$, 4.62 and 9.36 m, where X is the streamwise distance from the model's leading edge and X_i is the streamwise location of the injector slot. A known concentration of fluorescent dye (Rhodamine 6G, Sigma Chemical) was thoroughly mixed into the injected polymer. The dye-laden polymer was illuminated with a light sheet normal to the plate surface but parallel with the flow (i.e. parallel the x–y plane). Light sheets were formed from the beams of pulsed Nd-YAG lasers operating at the 532 nm wavelength and were measured to be $\sim$125 μm thick at the plate surface. The illuminated polymer was imaged with a high-resolution camera (LaVision Imager Pro) having a field of view approximately 5 mm (streamwise) $\times$ 2 mm (wall-normal). Periscope prisms protruding 5 mm from the test surface were used to collect and redirect the fluorescent light to the cameras that were housed in waterproof boxes within the test model. Each prism was located 40 mm from the light sheet. A long-pass optical filter was used to attenuate the 532 nm illumination light and collect only the Stokes-shifted light from the fluorescent dye. Finally, a pair of cylindrical lenses was used to stretch the wall-normal component of the images approximately by a factor of 2.5. Further details are provided in Winkel *et al.* (2006).

The PLIF measurements were calibrated using a clear-plastic box that was filled with solutions of known polymer and dye concentrations and fitted onto the plate surface, immersing the light sheet and collection optics. The fluorescent return from

https://doi.org/10.1017/S0022112008004874 Published online by Cambridge University Press

	X/L	$X - X_i$ m	U (m s^{-1}) ±1 %	Re_X × 10^6	δ_{99} (mm) ±10 %	Θ mm ±5 %	K' × 10^{10}	C_f ± 0.0001	u_τ (m s^{-1})	l_v (μm)	k^+
Injector	0.10	0	6.57	8.7	18	2.2	7.3	0.0024	0.23	4.4	0.1
			13.11	17	17	1.9	3.7	0.0022	0.43	2.3	0.2
			19.75	26	15	2.0	2.4	0.0021	0.63	1.6	0.3
Sensor 1	0.15	0.64	6.58	13	25	2.8	7.3	0.0023	0.22	4.5	0.1
MS1			13.13	26	23	2.6	3.7	0.0021	0.42	2.4	0.2
			19.78	39	21	2.1	2.4	0.0020	0.62	1.6	0.2
Sensor 2	0.26	2.09	6.60	23	38	4.0	7.2	0.0021	0.22	4.6	0.1
			13.18	45	35	3.6	3.6	0.0019	0.41	2.5	0.2
			19.85	67	34	3.6	2.4	0.0018	0.60	1.7	0.2
Sensor 3	0.46	4.62	**6.65**	40	**58**	**5.7**	7.2	0.0020	0.21	4.8	0.1
MS2			**13.25**	79	**55**	**5.3**	3.6	0.0018	0.40	2.5	0.2
			19.93	119	**54**	**5.2**	2.4	0.0017	0.58	1.7	0.2
Sensor 4	0.58	6.11	6.66	50	68	6.5	7.2	0.0019	0.21	4.8	0.1
			13.30	99	65	6.1	3.6	0.0017	0.39	2.5	0.2
			20.03	150	65	6.0	2.4	0.0017	0.58	1.7	0.2
Sensor 5	0.72	7.91	6.69	62	81	7.5	7.2	0.0019	0.20	4.9	0.1
			13.35	124	77	7.1	3.6	0.0017	0.39	2.6	0.2
			20.11	187	78	6.9	2.4	0.0016	0.58	1.7	0.2
Sensor 6	0.83	9.36	**6.70**	72	**90**	**8.2**	7.1	0.0018	0.20	5.0	0.1
MS3			**13.39**	144	**86**	**7.8**	3.6	0.0017	0.39	2.6	0.2
			20.22	217	**88**	**7.5**	2.4	0.0016	0.57	1.8	0.2

TABLE 1. Single phase free-stream velocity U, Reynolds number Re_X, 99 % boundary layer thickness δ_{99}, momentum thickness Θ, acceleration parameter K', skin-friction coefficient C_f, the friction velocity u_τ, the viscous length l_v and the surface roughness parameter k^+ at the downstream locations of the injector, the six skin-friction measurement balances and the three PLIF measurement stations. Bold values result from the measured velocity profiles.

the calibration solutions was used to relate the electrical signal from each imaging pixel with the dye concentration, accounting for spatial variations in recorded light sheet intensity. The calibration range for each PLIF station and the initial dye concentration in the injected polymer solution were chosen such that the PLIF measurement at a particular location produced sufficient signal-to-noise ratio. As the dilution ratio of injected polymer varied drastically along the test surface, it was usually not possible to select a single dye concentration that would result in acceptable results at all three PLIF locations, necessitating repeated tests with different dye concentrations. The uncertainty of the PLIF measurements varied with dilution, but is typically ±20 % for dilutions less than 100:1 and ±30 % for dilutions greater than 100:1.

3. Baseline flow results

The baseline flow measurements from this experiment are summarized in table 1 for the six skin-friction measurement locations ($X - X_i = 0.64$, 2.09, 4.62, 6.11, 7.91, 9.36 m). Boundary layer growth on the model and test section sidewalls caused a slight favourable pressure gradient; the nominal test speeds – 6.65, 13.2 and 19.9 m s^{-1} – are valid for the streamwise centre of the plate. Full baseline boundary layer profiles were measured with a laser Doppler velocimetry (LDV) system at the same locations as the third and sixth shear stress sensors. The local free stream velocity U, the 99 % boundary layer thickness δ_{99} and the momentum thickness Θ, inferred from these measurements are listed in bold in table 1. The remaining entries for U in table 1

https://doi.org/10.1017/S0022112008004874 Published online by Cambridge University Press

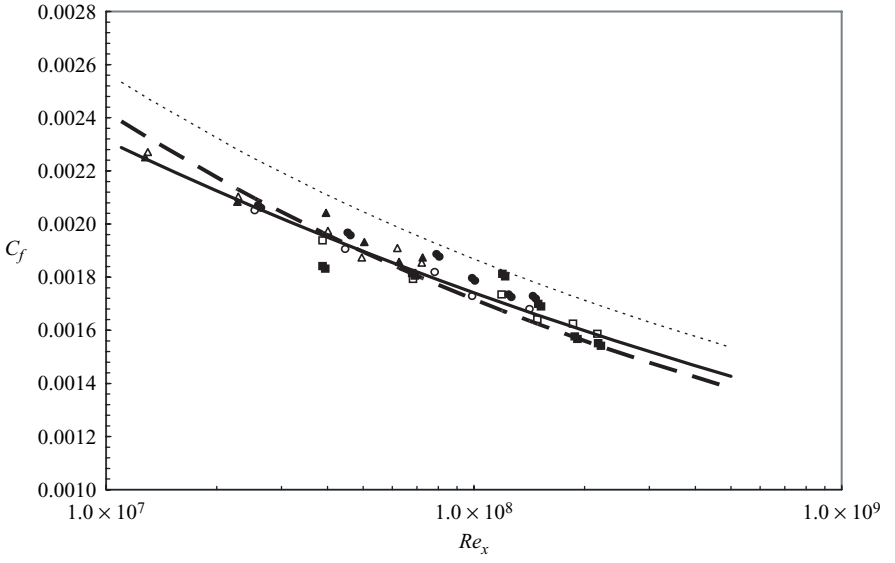


FIGURE 2. Baseline skin-friction coefficient, C_f, versus Reynolds number from two separate phases of the experiments (open symbols from Phase III and closed symbols from Phase IV) for $U = 6.65$ (△), 13.2 (○) and (□) 19.9 m s^{-1}. Also shown are the power-law fit to the experimental data ((3.1), solid line) and two standard skin-friction correlations from White (1991; light dashed line) and Schultz-Grunow (1941; heavy dashed line).

were inferred from static pressure measurements made along the plate and the steady Bernoulli equation. The remaining entries for δ_{99} and Θ in table 1 were obtained from simple power-law fits to the LDV-profile-determined values of δ_{99} and Θ and are within a few percent of the values obtained from standard flat-plate TBL formulae. In addition, table 1 provides values for the downstream-distance-based Reynolds number $Re_x = Ux/\nu$, the skin-friction coefficient $C_f = \tau_w/(1/2)\rho U^2$, the acceleration parameter $K' = (\nu/U^2)(\mathrm{d}U/\mathrm{d}x)$, the friction velocity $u_\tau = (\tau_w/\rho)^{1/2}$, the viscous length $l_\nu = \nu/u_\tau$ and the ratio k^+ of the test-surface roughness height divided by the viscous length l_ν. When $K' < 10^{-6}$, flow acceleration should be sufficiently mild so that there will be little or no deviation in the boundary layer's profile from the typical log law (Patel 1965); for the current experiments, $K' < 10^{-9}$ and when $k^+ \leqslant 1$ or so, the plate surface can be considered hydrodynamically smooth.

Baseline skin-friction coefficients are shown in figure 2 with the standard friction correlations of White (2005) and Schultz-Grunow (1941). Skin-friction results from two separate tests conducted a year apart are provided to show the repeatability of the measurements. The measured skin-friction agrees with the Schultz-Grunow correlation and a simple power-law fit (solid line) to the experimental data taken at the time of the polymer tests (open symbols) is

$$C_f = (0.0170 \pm 0.0004) Re_x^{-(0.1237 \pm 0.0067)}. \tag{3.1}$$

4. Polymer solution rheology

The rheology of high molar mass aqueous PEO solutions and the molecular interactions with turbulent flow are complex and continue to be an active area of investigation (Kalashnikov, 1994; Vlassopoulous & Schowalter 1994; Tirtaatmadja, McKinley & Cooper-White 2006). Numerical simulations of polymer-laden turbulent

https://doi.org/10.1017/S0022112008004874 Published online by Cambridge University Press

PEO polymer	M_w (g mol^{-1})	$[\eta]_o$ (cm^3 g^{-1})	c^* (w.p.p.m.)	Δ/C (w.p.p.m.$^{-1}$)	θ_Z (s)	$\theta_K/C^{1/2}$ (s)	γ^* (s^{-1})	γ_D (s^{-1})
WSR-N60K	2.3×10^6	1.1×10^3	8.7×10^2	4.4×10^2	4.6×10^{-4}	1.30	1.5×10^3	2.4×10^4
WSR-301	4×10^6	1.8×10^3	5.7×10^2	8.1×10^2	1.2×10^{-3}	2.17	8.4×10^2	7.1×10^3
WSR-308	8×10^6	3.0×10^3	3.3×10^2	1.7×10^3	4.2×10^{-3}	3.58	4.2×10^2	1.5×10^3

TABLE 2. Polymer solution properties.

flow have attempted to capture the polymer-turbulence interactions by means of various polymer-flow constitutive models. For example, the FENE-P (Finite Elastic Non-Linear Extensible-Peterlin) dumbbell constitutive model has been widely used because it incorporates the rheological effects of polymer finite extensibility and is computationally efficient (Beris & Dimitropoulos 1999; Housiadas & Beris 2003; Dubief *et al.* 2004; Almeida *et al.* 2006). Formally, the FENE dumbbell models are appropriate as a molecular description of dilute polymer solutions below the overlap concentration c^*. This dilute limit for polymer solutions is determined from a common definition of c^*:

$$c^* = 1/[\eta]_o. \tag{4.1}$$

The intrinsic viscosity $[\eta]_o$ of PEO solutions (unit: cm^3 g^{-1}) can be determined from M_w using the Mark–Houwink relationship provided by Bailey and Callard (1959):

$$[\eta]_o = 0.0125 M_w^{0.78}. \tag{4.2}$$

Values of c^* and $[\eta]_o$, for the three PEO solutions of the current study are provided in table 2. In the current study, all concentrations of injected polymer solutions lie above the overlap concentration. Thus, the TBL-flow measurements presented here are likely beyond the range of current computational predictions until some distance downstream of the injector where the polymer concentration drops below c^*.

Even though exhaustive correlation of PDR to polymer solution rheological properties was beyond the scope of this investigation, rheological parameters of the injected solutions are provided in table 2, including Δ/C a relationship between the limiting shear viscosities at zero and infinite shear (Kalashnikov 1998); an expression for the relaxation time, the Zimm time θ_Z, which should be used for very low concentrations where R is the ideal gas constant (Dealy & Larson 2006); a relationship for the minimum shear rate for drag reduction onset γ^* (Vanapalli *et al.* 2005) derived from the data provided by Virk (1975), and the critical shear rate for degradation γ_D of PEO solutions (Vanapalli *et al.* 2005) where M_w is the molecular weight in g mol^{-1} and γ_D is in s^{-1}:

$$\Delta = \left[\left(\frac{[\eta]_o}{136.6}\right)^2 + 0.434[\eta]_o - 126\right] C, \tag{4.3}$$

$$\theta_K = \left[\frac{[\eta]_o}{549.5} - \left(\frac{[\eta]_o}{3255}\right)^3 - 0.51\right] \mathrm{e}^{-(T_c/50)^2} C^{1/2}, \tag{4.4}$$

$$\theta_Z = 0.422 \frac{[\eta]_o M_w \eta_S}{RT}, \tag{4.5}$$

$$\gamma^* = (3.35 \times 10^9) M_w^{-1}, \tag{4.6}$$

$$\gamma_D = 3.23 \times 10^{18} \times M_w^{-2.20}. \tag{4.7}$$

https://doi.org/10.1017/S0022112008004874 Published online by Cambridge University Press

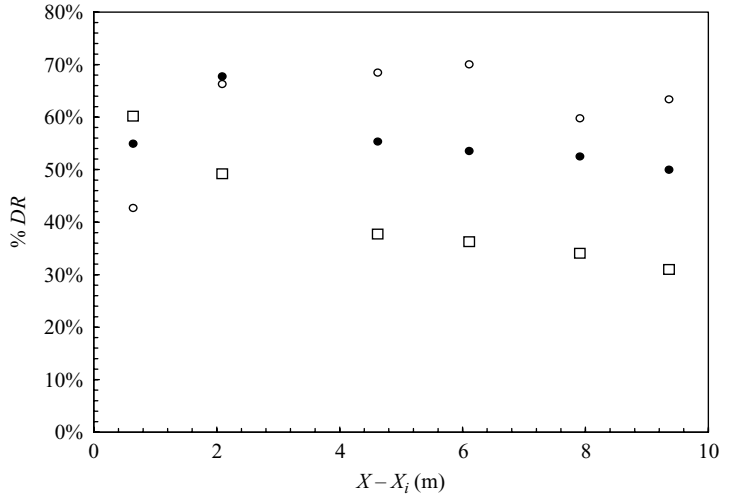


FIGURE 3. The $\%DR$ versus downstream distance from the injector, $X - X_i$, for WSR-308 for $C_i = 4000$ w.p.p.m. polymer injected at $Q_i/Q_S = 10$ for $U = 6.65$ (○), 13.2 (●) and 19.9 m s^{-1} (□).

Here, (4.7) is a best fit to the PEO data in figure 6 of Vanapalli *et al.* (2005). A potential complication of assessing drag reduction based solely on polymer rheology is that the treatments discussed above are applicable to polymer chains described by a well-characterized molar mass. However, as discussed in the literature, high-molar-mass PEO is susceptible to intermolecular aggregation in aqueous solution (Dunlop & Cox 1977; Polverari & van de Ven 1996; Faraone *et al.* 1999; Ho, Hammouda & Kline 2003).

5. Drag reduction resulting from polymer injection

5.1. *Stages of polymer mixing*

Injection of polymer solution into the TBL results in a distribution of polymer across the boundary layer that evolves in the streamwise direction. Poreh & Hsu (1972) describe four mixing regions: initial, intermediate, transition and final. In the initial region, the injected polymer lies within the sub-layer. In the intermediate region, the polymer lies within a layer thinner than the boundary layer thickness but thicker than the viscous sub-layer and buffer layer. In the transition region, the polymer is diffused throughout most of the TBL. In the final region, the growth rate and thickness of the polymer-laden portion of the TBL is the same as that of the TBL itself. This process can be compared to the similarly defined mixing regions of a passive scalar, discussed by Poreh & Cermack (1964). In the current experiments, the injected polymer flux is larger than Q_S, and therefore it is artificial to distinguish the initial and intermediate stages, which herein are combined and referred to as the development region. Although these stages are defined for the mixing process, PDR has a corresponding character in each.

5.2. *Peak drag reduction*

The highest observed levels of PDR occurred with the highest polymer flux ($C_i = 4000$ w.p.p.m., $Q_i = 10\,Q_s$) of the highest M_w polymer (WSR-308). These are 70, 67 and 60 $\%DR$ at 6.65, 13.2 and 19.9 m s^{-1}, respectively, as shown in figure 3. The

https://doi.org/10.1017/S0022112008004874 Published online by Cambridge University Press

peak $\%DR$ was observed at the first measurement station ($X - X_i = 0.64$ m) only at 19.9 m s^{-1}, whereas peak drag reductions occurred at $X - X_i$ of approximately 6 and 2 m at 6.65 and 13.2 m s^{-1}, respectively. The peak $\%DR$ observed in these experiments agrees with prior work; Vdovin & Smol'yakov (1981) report maximums between 65 and 70 $\%DR$ and Petrie & Fontaine (1996) report maximums between 64 and 67 $\%DR$ for WSR-301. Yet the peak $\%DR$ values are slightly lower than those predicted by Virk, Mickley & Smith (1970) for uniform concentration TBL flow. The peak $\%DR$ observed at 6.65, 13.2 and 19.9 m s^{-1} for the two lower M_w polymers were 70, 64 and 57 $\%DR$ and 52, 55 and 57 $\%DR$, for WSR-301 and WSR-N60K, respectively. It is interesting to note that the lowest M_w polymer (WSR-N60K) is the only one where peak $\%DR$ actually increases with increase in free stream speed.

5.3. *K-factor scaling of the drag reduction*

A simple scaling relationship that led to a reasonable collapse of PDR data was developed by Vdovin & Smol'yakov (1981). Their parameter K is given by

$$K = Q_i C_i / K = Q_i C_i / \rho (X - X_i) U. \tag{5.1}$$

When $\%DR$ is graphed versus K, the intermediate region shows a logarithmic decrease in drag reduction with decreasing K (i.e. increasing X after fixing the other variables). Poreh & Hsu (1972) demonstrate that such behaviour can be explained using a Lagrangian similarity hypothesis for mixing of the polymer in the logarithmic layer of the TBL, as first proposed by Batchelor (1957). The rate of mixing is related to the local friction velocity that, in turn, is a function of the near-wall polymer concentration. However, the mixing rate is not expected to be a simple logarithmic relationship. Nevertheless, the K-scaling is a simple and useful way of organizing, comparing and revealing features of $\%DR$ data. Yet, some caution should be exercised when using K-scaling to predict PDR levels far beyond the parameters of the original experiments.

Figure 4 presents $\%DR$ versus K for the three polymers used. The development region is evident for higher values of K (e.g. the measurements closest to the injector). The $\%DR$ increases and reaches a maximum near $K \sim 2 \times 10^{-7}$, then decreases with decreasing K value (e.g. increasing distance from the injector). The product $Q_i C_i$ adequately collapses the data for a given speed, suggesting that it is the total flux of polymer that is the relevant quantity over the range of variables of these tests, an observation that agrees with Vdovin & Smol'yakov (1978, 1981). In contrast, Warholic *et al.* (1999) suggest that for equivalent polymer fluxes, lower injection rates of higher concentration solution, where aggregation is more likely to occur, will result in higher $\%DR$. In their experiments, equivalent fluxes of polymer at 500 and 100 w.p.p.m. produced 45 and 19 $\%DR$, respectively. Since the experiments of Warholic *et al.* (1999) were performed in a relatively slow channel flow at speeds up to 2 m s^{-1}, the role of aggregation may have been more pronounced. Results from the present experiment are shown in figure 5 for two pairs of equivalent fluxes of WSR-301 at two concentrations that differ by a factor of two and both concentrations exceed c^*. The concentrations of Warholic *et al.* were lower and also differed by a factor of five.

Figure 4 shows a potentially important trend that has not been reported in prior PDR studies, segregation of $\%DR$ versus K in the transition region according to free stream speed for the WSR-301 and WSR-308 polymers. For equivalent K values in the transition region, the level of observed drag reduction decreases with increasing free stream speed. The fact that this speed dependence is only observed for the WSR-301 and WSR-308 indicates that polymer chain-scission may be occurring. The wall-shear

https://doi.org/10.1017/S0022112008004874 Published online by Cambridge University Press

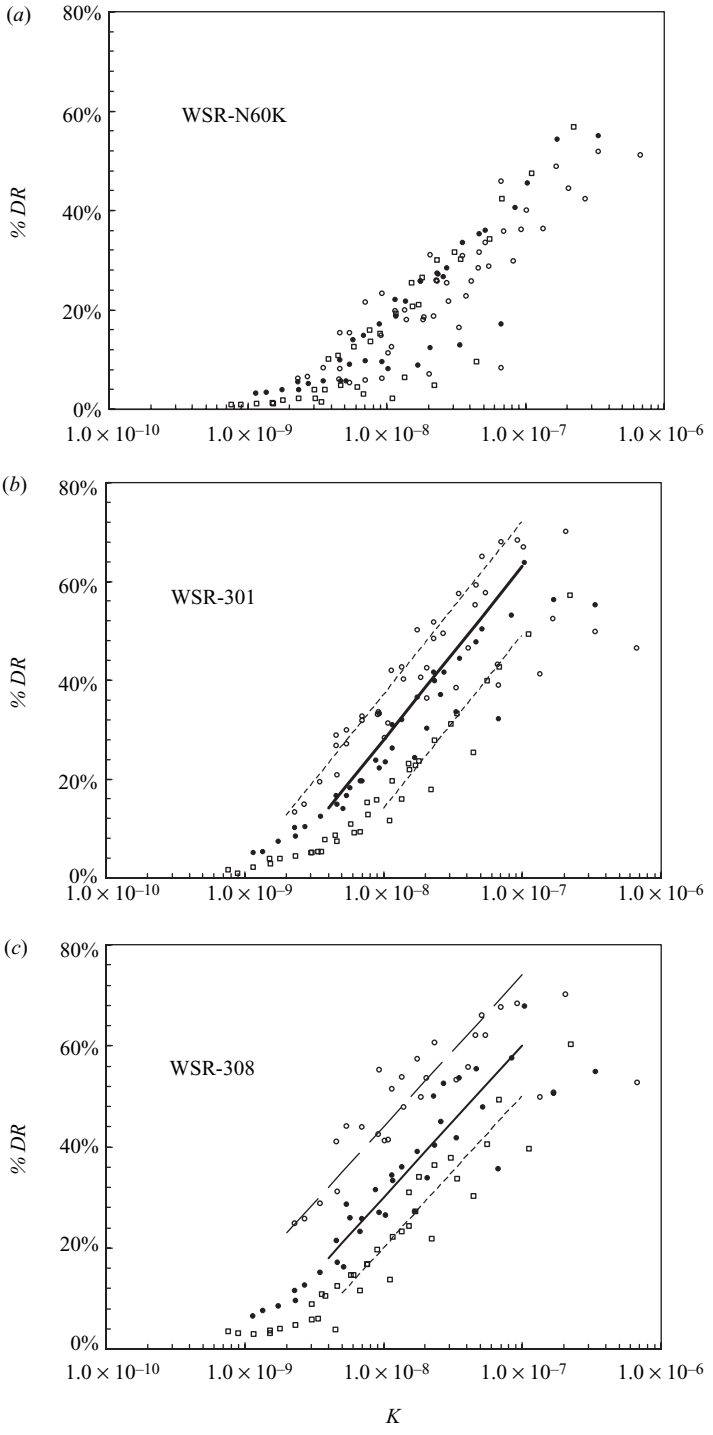


FIGURE 4. %DR versus K for all three M_w polymers at $U = 6.65$ (○), 13.2 (●) and 19.9 (□) m s^{-1}. Shown in (b) and (c) are trend lines for the %DR versus K relationships demonstrating the speed dependence (dashed lines) in the transitional regime. Also shown in (b) is the trend line reported by Vdovin & Smol'yakov (1981) for the transitional region (solid line).

https://doi.org/10.1017/S0022112008004874 Published online by Cambridge University Press

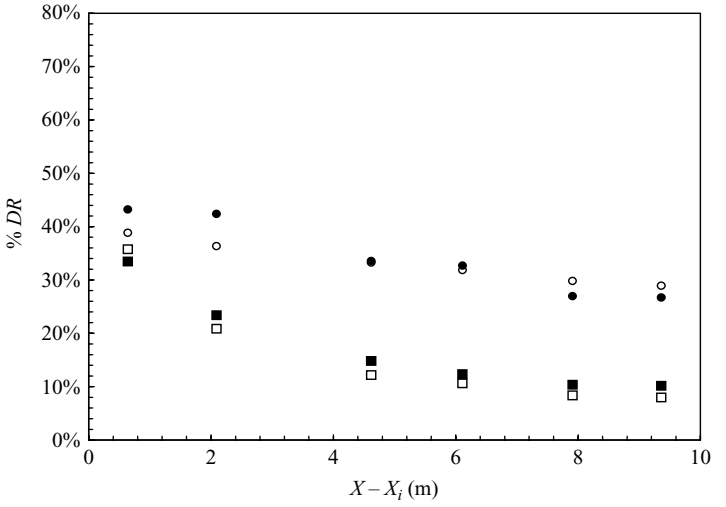


FIGURE 5. The $\%DR$ versus downstream distance from the injector, $X - X_i$, for WSR-301. (○) $U = 6.65\,\mathrm{m\,s^{-1}}$, $C_i = 1000$ w.p.p.m. and $Q_i/Q_S = 4$; (●) $U = 6.65\,\mathrm{m\,s^{-1}}$, $C_i = 2000$ w.p.p.m. and $Q_i/Q_S = 2$; (□) $U = 13.2\,\mathrm{m\,s^{-1}}$, $C_i = 1000$ w.p.p.m. and $Q_i/Q_S = 4$; (■) $U = 13.2\,\mathrm{m\,s^{-1}}$, $C_i = 2000$ w.p.p.m. and $Q_i/Q_S = 2$. The open and closed circles fall together and correspond to the same product $Q_i C_i$ but different values of Q_i and C_i. The same is true of the open and closed squares.

rates at injection are of the order of 5×10^4, 2×10^5 and $4 \times 10^5\ \mathrm{s^{-1}}$ for 6.65, 13.2 and $19.9\,\mathrm{m\,s^{-1}}$, respectively, and (4.7) predicts polymer chains with M_w above 1.9, 1.0 and 0.7 million will be susceptible to degradation at these three shear rates. Thus, some degree of polymer degradation is possible at all test speeds. In addition, aggregation may contribute to the speed dependence, as aggregation is more likely to occur with the higher M_w polymers. Speed-based fits to $\%DR$ versus K in figures 5(*b*) and 5(*c*) demonstrate that the overall slope in the transition region is similar for each of the three speeds, despite the observed speed dependence. Also plotted is a line (bold) representing the best-fit slope for the transitional regime reported by Vdovin & Smol'yakov (1981) for WSR-301, and the current $13.2\,\mathrm{m\,s^{-1}}$ data agree with it well. Vdovin & Smol'yakov (1981) do not distinguish their $\%DR$ data with specific injection conditions and free stream speed. Yet, their data are similar to the current 6.65 and $13.2\,\mathrm{m\,s^{-1}}$ data in slope, maximum $\%DR$ and K value for the beginning of the transition region.

Examination of other published PDR results for WSR-301 also shows some flow-speed variability although the trend is somewhat masked by scatter. Table 3 lists the details of several experiments and figure 6 presents WSR-301 $\%DR$ versus K from them, sorted into low-speed (6*a*), medium-speed (6*b*) and high-speed (6*c*) results. Here, the upper envelope of the $\%DR$ versus K data moves downward and to the left with increasing flow speed. The considerable data spread in the three frames of figure 6 might be partially explained by experimental differences. In the studies of Fontaine *et al.* (1992) and Petrie *et al.* (2003), a relatively large drag balance was employed that could mask the initial region and peak level of drag reduction. In addition, their injectors spanned only the middle 50 % of their test plate and this may have induced unintended three-dimensional effects. The low-speed data (figure 6*a*) are most scattered. Here the role of aggregation, as presented by Warholic *et al.*

https://doi.org/10.1017/S0022112008004874 Published online by Cambridge University Press

https://doi.org/10.1017/S0022112008004874 Published online by Cambridge University Press

	TBL thickness at injector (mm)	Maximum measurement distance from the injector (m)	Speed Range ($m\,s^{-1}$)	Conc. Range (w.p.p.m.)	Q_i/Q_s	Balance Type	Injector Type	Injector Span (% of total)	X_D $K=2\times10^{-7}$ $U=6.7\,m\,s^{-1}$ (m)	X_D $K=2\times10^{-7}$ $U=20\,m\,s^{-1}$ (m)
Vdovin and Smol'yakov (1981)	8 to 50	4.375	2.5 to 10	250 to 4000	1.1 to 23	Local (20 mm × 20 mm)	20 degree slot (0.4 × 140 mm or 0.8 × 140 mm)	87 %	0.02 to 5.16	0.01 to 1.72
Fontaine *et al.* (1992)	∼4*	0.36 to balance trailing edge	4.5 to 18.3	500 and 1000	1.6 to 4	Integrated (318 × 152 mm)	25 degree slot (1 mm × 152 mm)	50 %	0.05 to 0.22	0.02 to 0.08
Petrie *et al.* (1996)	∼10 to ∼20**	1.87	7.6 to 16.8	500 to 2000	2.5 to 10	Local (38 × 127 mm)	25 degree slot (2.5 mm × 610 mm)	50 %	0.07 to 1.12	0.02 to 0.37
Petrie *et al.* (2003)	∼4*	0.38 to balance trailing edge	4.57 to 13.7	200 to 2000	2 to 20	Integrated (318 × 152 mm)	Contoured Plenum Slot	81 %	0.02 to 2.24	0.01 to 0.75
Petrie *et al.* (2005)	∼4*	0.33	6 to 18	100 to 500	2 to 20	Local (38 × 127)	Contoured Plenum Slot	81 %	0.01 to 0.56	0.00 to 0.19
Present results	16 to 20	9.36	6.6 to 20	1000 to 4000	2 to 10	Local (152.4 mm diameter)	25 degree slot (1 mm exit cross section × 2650 mm)	88 %	0.11 to 2.04	0.04 to 0.75

*reported by Madavan *et al.* (1985); ** estimated assuming the origin of the TBL is the model leading edge.

TABLE 3. Experimental set-up and conditions of previous experiments reporting drag reduction *versus* *K*-factor for line-source injection into a turbulent boundary layer using WSR-301.

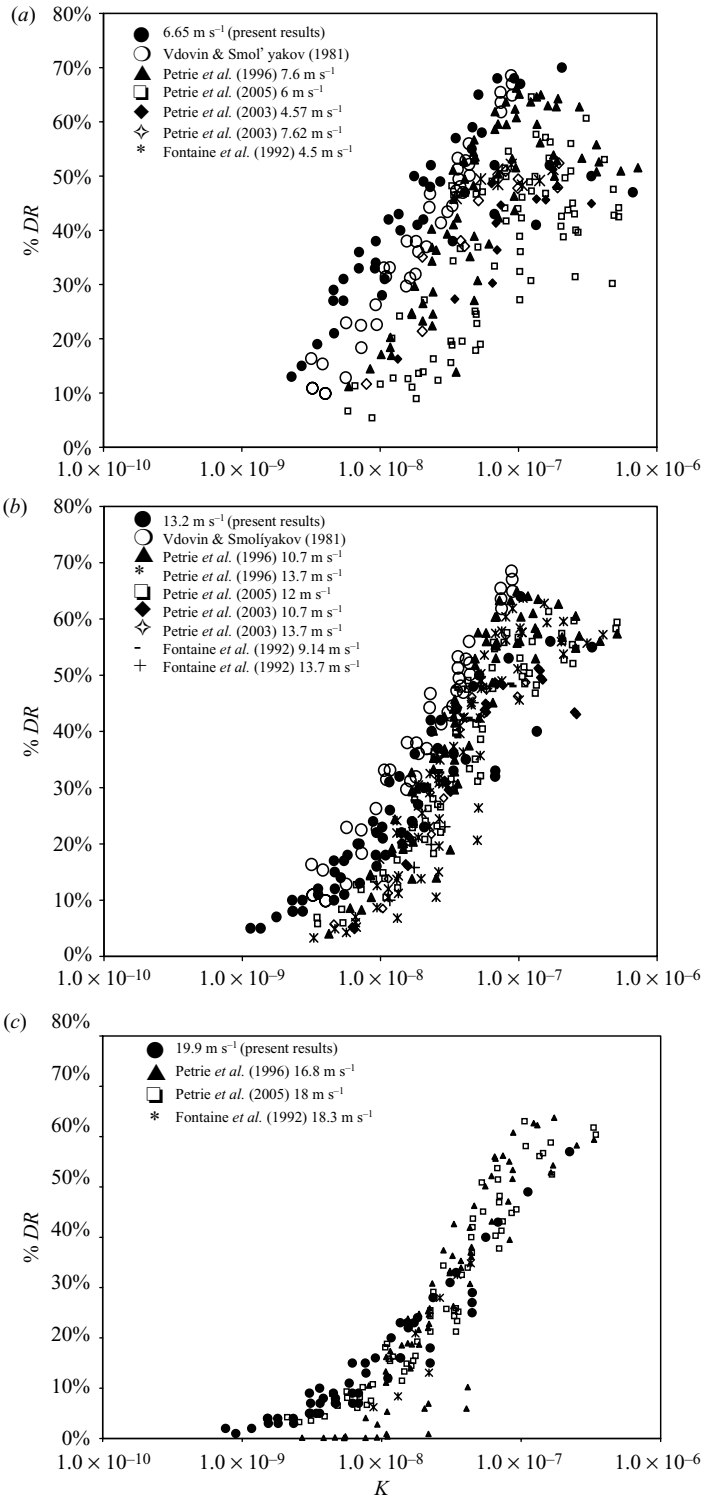


FIGURE 6. K versus $\%DR$ from the present experiments and those reported previously for WSR-301. Data are segregated into (*a*) low, (*b*) medium and (*c*) high free-stream speeds. The experimental descriptions and conditions are provided in table 3.

https://doi.org/10.1017/S0022112008004874 Published online by Cambridge University Press

(1999), may be an additional factor contributing to the scatter. Interesting results for the physical length of the development region in the present and previous experiments are hidden in the data shown in figures 5 and 6. In the present experiments, for any particular set of parameters, the PDR peak usually occurred between the injector and the second skin-friction sensor at $X - X_i = 2.09$ m. Table 3 provides a list of the ranges of lengths of the development region X_D defined as the distance between the injection and the location where $K = 2 \times 10^{-7}$, for the range of $Q_i C_i$ in each experiment at $U = \sim 7$ and $\sim 20\,\mathrm{m\,s^{-1}}$. For the smaller scale experiments, it is often not possible to determine the development region length at the lower speeds since X_D can extend beyond the farthest measurement location. In the present experiment, X_D is the largest at the lowest speed and highest $Q_i C_i$, and this distance is comparable to the experiments of Vdovin & Smol'yakov (1981) and about a metre longer than that reported by Petrie *et al.* (1996). At the highest free stream speeds, X_D is reduced, and there is less spread in the $\%DR$ versus K data from the different experiments.

The $\%DR$ versus K plots also reveal the end of the transition region and the start of the final mixing region, beyond which the polymer fills the boundary layer and mixes at a rate similar to that of a passive scalar. Here, the $\%DR$ has decreased to less than 20 %. The K value at which transition to the final zone mixing occurs varies with both free stream speed and M_w, but is generally in the range $2 \times 10^{-9} < K < 6 \times 10^{-9}$, with lower K values corresponding to higher M_w and lower free stream speed. Variation in the geometry of the injection slots used in these studies as well as variation in the exit velocity of the injected polymer (typically 1 %–10 % of the free stream speed) did not appear to strongly influence the length of any of the three mixing regions.

5.4. *Drag reduction in the development region*

The concentration needed to reach the MDR asymptote in internal flows of aqueous PEO solutions lies in the range of 10–100 w.p.p.m. depending on topology, Reynolds number and polymer molecular weight. Consequently, it was expected that an external boundary layer flow would reach, and perhaps even persist at, the MDR asymptote if PEO was injected at concentrations at or above 1000 w.p.p.m.. However, in the present experiments, MDR was not routinely achieved, even in the development region near the injector, and if the flow did approach MDR, this level of drag reduction did not persist. Instead, drag reduction was found to increase with downstream distance in the development region when this region extended over two or more shear stress sensors, a phenomenon also noted in Petrie *et al.* (1996, 2005). As stated above, X_D is roughly proportional to $Q_i C_i / U$ but it also increases with M_w. Unfortunately, the phenomena leading to the increase in $\%DR$ in the development region are not readily understood. Polymer concentration-field measurements (see § 6.3) are highly variable in the development region and are sometimes nearly binary between zero and C_i. The elasticity, shear thinning viscosity and high extensional viscosity of the polymer solution, along with the boundary layer turbulence are likely contributors to these fluctuations. Here, the polymer forms into long high-concentration filaments as it is drawn from the injector slot by the fast-moving boundary layer flow; it does not exit the injection slot in a two-dimensional sheet.

An explanation of the increasing $\%DR$ with downstream distance in the development region remains elusive yet it may be attributed to a few phenomena. First, as the polymer mixture is non-uniform, regions of high $\%DR$ may exist with regions of essentially zero $\%DR$, resulting in a lower average $\%DR$. As the polymer concentration of the interstitial fluid between filaments increases with downstream mixing, the corresponding average $\%DR$ increases. Second, for the polymers to

https://doi.org/10.1017/S0022112008004874 Published online by Cambridge University Press

effectively modify turbulence and reduce drag, they must mix through the buffer layer and a finite time (or distance) is required for this wall-normal transport. And finally, the injected polymer solutions have relaxation times of the order of 0.1 s. Thus, a non-zero extent of streamwise flow may be needed for the polymers to stretch, and interact with the TBL turbulence. Consequently, the peak $\%DR$ in any experiment may occur some distance, perhaps as much as several metres, downstream of the injector.

5.5. *Drag reduction in the transitional and final regions*

The transitional mixing region, which starts at the location of peak $\%DR$, is characterized by a logarithmic decrease in $\%DR$. In this region, the near-wall concentrations have typically been reduced on the order of 100-fold relative to that of the injection concentration, and polymer has mixed throughout most of the TBL. In the transitional mixing region, the polymer filaments observed in the development region are much less pronounced and the polymer concentration field is much more uniform. The final region of mixing following the transitional region is characterized by low levels of drag reduction, absence of all polymer filaments and polymer mixed across the entire boundary layer. While substantial levels of $\%DR$ ($>20\,\%$) are lost by the final region, the decay rate is much less precipitous than that in the transitional region. The K values where the transitional region and final regions intersect varies with free stream speed and M_w, but typically are of the order of $2 \times 10^{-9} < K < 6 \times 10^{-9}$.

6. Evolution of the near-wall polymer concentration

6.1. *Near-wall polymer concentration profiles*

Measurements of the polymer concentration were made in the near-wall region at three streamwise locations using PLIF. Examples of wall-normal profiles of the polymer at $X - X_i = 0.64$ and 4.62 m are shown in figure 7 for WSR-301, 6.65 m s^{-1} and $Q_i = 10Q_S$. The sharpest concentration gradients near the wall occur at the first measurement station. Note that the peak polymer concentration at $X - X_i = 0.64$ m does not occur at the wall, but at 100 or 200 microns above it. This phenomenon was observed only at this location at the lowest test speed. While an unintended artefact of the optical train may be suspected for this anomaly, this was not observed in the calibrations performed with uniform polymer–dye concentrations. Moreover, this phenomenon has also been observed by Brungart *et al.* (1991). They found peak concentrations occurred at $10 < y^+ < 50$ from the wall 0.12 m from the injector at 4.6 m s^{-1}. However, they ascribe this result to the varying index of refraction with polymer concentration. Another possibility lies in a flow morphology composed of lifted strands of concentrated polymer. Unfortunately, the three-dimensional flow interrogation necessary to resolve this issue was beyond the scope of these experiments. At the second and third measurement stations, the concentration profiles are much smoother and nearly uniform over the measurement volume $0 < y < 2$ mm. For diffusion analysis, the maximum concentration is used; it is often, but not necessarily, the wall concentration.

Vdovin & Smol'yakov (1978, 1981), Fontaine *et al.* (1992) and Petrie *et al.* (1996, 2005) measured concentration across the boundary layer and discuss the evolution of the diffusion-zone 50 % thickness (λ), relative to the boundary layer thickness, λ/δ_{99}, as a function of downstream distance from the point of injection. Sommer & Petrie (1992) also discuss the evolution of the concentration profile, $C(y)/c_M$, within the different mixing zones, where c_M is the maximum concentration in the near-wall region. The concentration measurements of the present experiments were made only

https://doi.org/10.1017/S0022112008004874 Published online by Cambridge University Press

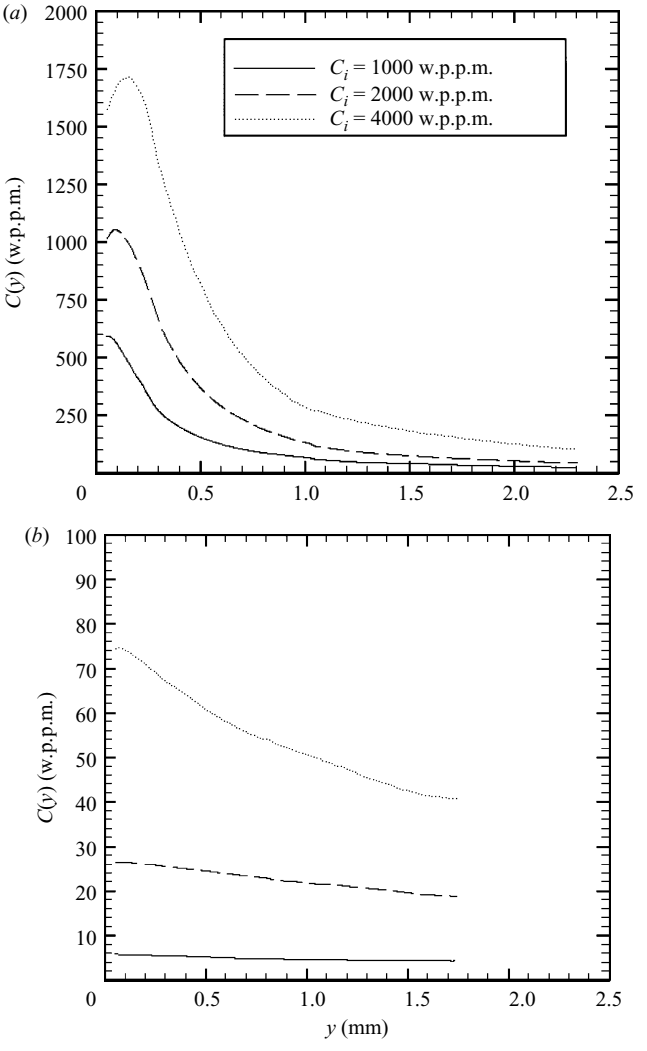


FIGURE 7. Near-wall concentration profiles of WSR-301 at $X - X_i = 0.64$ m (a) and 4.62 m (b) for $U = 6.65\,\mathrm{m\,s^{-1}}$ and $Q_i/Q_S = 10$.

in the near-wall region and in most cases the 50 % diffusion layer thickness cannot be identified, so the current data cannot be presented in the same manner.

6.2. *Near-wall concentration versus K*

The maximum polymer concentration is presented as a function of K in figure 8 (the data for WSR-N60K also include data presented by Petrie *et al.* 2005). As expected, the near-wall concentration is reduced as K is reduced (e.g. as the distance from the injection location increases). This scaling produces a reasonable collapse of c_M from the current experiment. Experimental differences may be the reason for the lack of collapse with the WSR-N60K data of Petrie *et al.* (2005). Nevertheless, there is little difference in the K-factor scaling of c_M with various M_w polymers. Most of the data collected at the second and third measurement stations are in the transitional and final mixing zones, while a few data points are collected in the development region. There is considerable scatter in the data, but the WSR-301 and -308 data consistently

https://doi.org/10.1017/S0022112008004874 Published online by Cambridge University Press

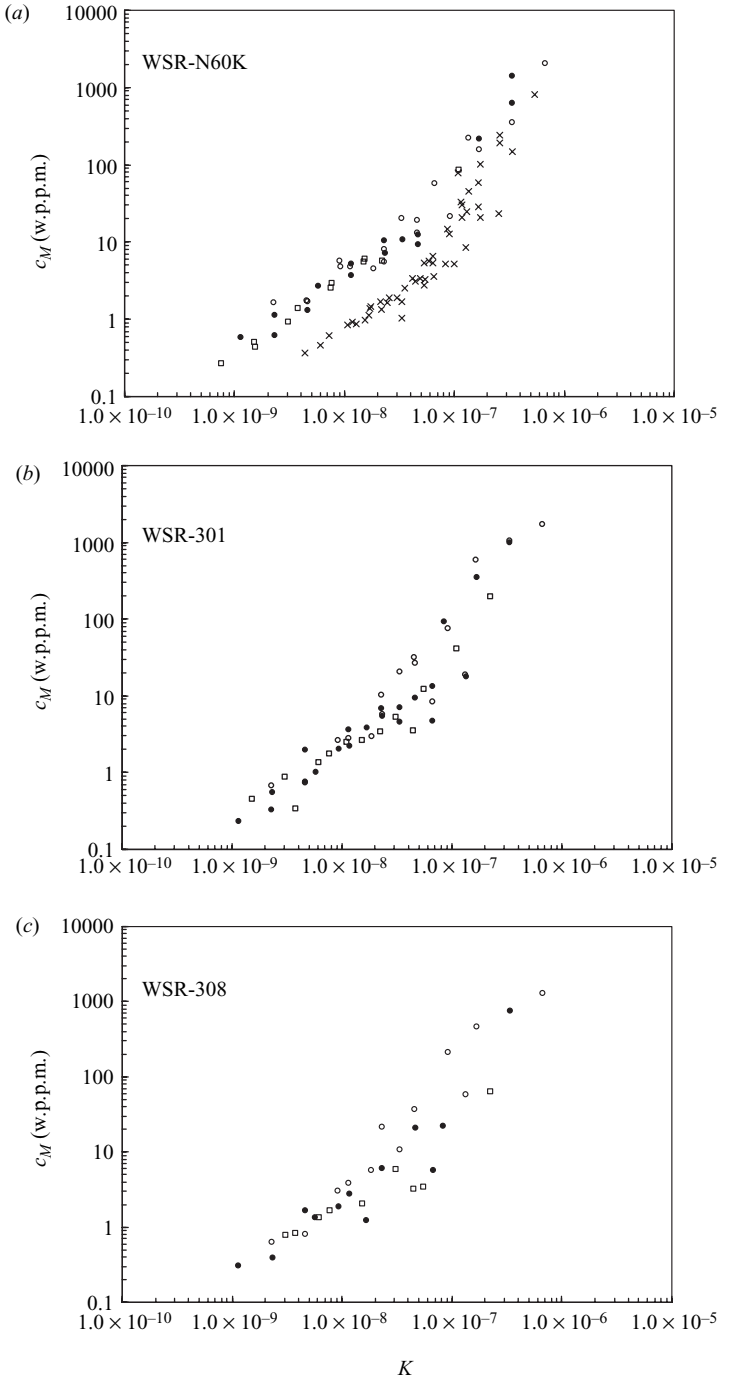


FIGURE 8. The maximum near-wall concentration, c_M, versus K for (*a*) WSR-N60K, (*b*) WSR-301 and (*c*) WSR-308 at $U = 6.65$ (○), 13.2 (●) and 19.9 (□) m s^{-1}. The data for WSR-N60K from Petrie *et al.* (2005) are also included (×).

https://doi.org/10.1017/S0022112008004874 Published online by Cambridge University Press

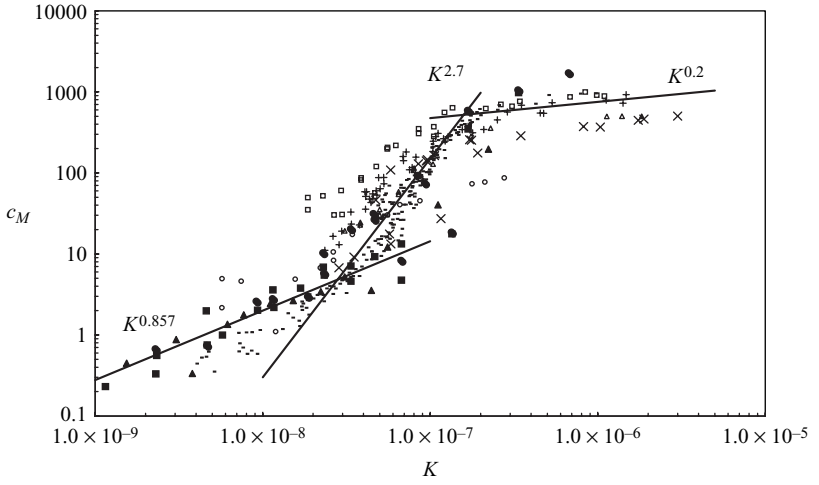


FIGURE 9. The values of c_M versus K for WSR-301 of the present experiment: $U = 6.65$ (●), 13.2 (■) and 19.9 (▲) m s^{-1} with previously reported results; Fruman & Tulin (1976) with $C_i = 100$ w.p.p.m. (○), 500 w.p.p.m. (△) and 1000 w.p.p.m. (□); Vdovin & Smol'yakov (1978), assuming $C_i = 1000$ w.p.p.m. (+); Vdovin & Smol'yakov (1981), assuming $C_i = 1000$ w.p.p.m.; (−); Fontaine *et al.* (1992) (×). The three lines correspond to exponents of 0.2, 2.7 and 0.857. Details of the previous experiments are provided in table 4.

suggest that, with increasing speed, c_M is reduced for a given value of K which supports the observed speed dependence in $\%DR$ versus K.

Figure 9 presents c_M versus K for the WSR-301 polymer from the present experiments along with previously reported results of Fruman & Tulin (1976), Vdovin & Smol'yakov (1978, 1981), Fontaine *et al.* (1992) and Petrie *et al.* (2005). The details of the prior studies are presented in table 4, where dye was mixed into the injected polymer and polymer concentration was inferred from the dye concentration. However, in the first three references, the near-wall flow was physically drawn from the test model and piped to a concentration measurement system. Fruman & Tulin (1976) discuss the proper selection of sampling flux, since it is important that only the near-wall fluid be sampled. However, even if the proper sampling flux is prescribed, it is possible to erroneously sample the polymer solution, since the solution is highly non-Newtonian (Lotto & El Riedy 1981). Hence, these measurements of wall concentration are potentially less certain than those resulting from direct *in situ* PLIF interrogation. Moreover, it is unclear how Fruman & Tulin (1976) managed the build-up of background polymer and dye in their experiment. Nevertheless, these measurements are included for completeness.

The three regimes of polymer mixing can be identified in figure 9. The development region is characterized by a wall concentration that is decreasing approximately as $K^{0.2}$. Over a range of $1 \times 10^{-7} < K < 2 \times 10^{-7}$, the wall concentration of the polymer begins to decrease at a much faster rate of $K^{2.7}$. This is the transitional mixing regime where the polymer is being mixed across the TBL. Once fully mixed across the TBL, the polymer is much more dilute and $\%DR$ consequently is reduced. In the final mixing region, the near-wall concentration reduces at the rate of TBL growth, $\sim K^{6/7}$, since $\delta_{99} \sim x^{6/7}$ (White 2005). The data in figure 9 are scattered, but the overall trends and dilution rates are similar. The data of Fruman & Tulin (1976) lie outside the general envelope of the data from more recent experiments, but it should be noted

https://doi.org/10.1017/S0022112008004874 Published online by Cambridge University Press

https://doi.org/10.1017/S0022112008004874 Published online by Cambridge University Press

	Maximum measurement distance from the injector (m)	Speed range ($m\,s^{-1}$)	Conc. Range (w.p.p.m.)	Q_i/Q_s	Measurement Method	Injector Type	Injector Span (% of total)
Fruman and Tulin (1976)	2.337	10.65	100 to 1000	11.2 to 27.3	Sampling Slits 38 mm × 0.25 mm	0 degree slot (0.5 × 300 mm)	∼100%
Vdovin and Smol'yakov (1978)	0.557	2 to 12	560 to 5000	1.3 to 12.6	Sampling Ports 0.5 mm diameter and Traversed Sampling Tubes with 0.15 × 1.5 mm openings	7 degree slot (0.7 × 120)	80 %
Vdovin and Smol'yakov (1981)	4.5	2.5 to 10	250 to 4000	1.1 to 23	Sampling Ports	20 degree slot (0.4 × 140 mm or 0.8 × 140 mm)	87 %
Fontaine *et al.* (1992)	∼0.3	4.5 to 18.3	500 and 1000	1.6 to 4	PLIF	25 degree slot (1 mm × 152 mm)	50 %
Petrie *et al.* (2005)	∼0.3	6 to 18	100 to 500	2 to 20	PLIF	Contoured Plenum Slot	81 %
Present results	9.36	6.6 to 20	1000 to 4000	2 to 10	PLIF	25 degree slot (1 mm exit cross section × 2650 mm)	88 %

TABLE 4. Experimental set-up and conditions of previous experiments reporting near-wall concentration measurements for line-source injection into a turbulent boundary layer, using WSR-301 and WSR-N60K (present results and Petrie *et al.*, 2005).

that these experiments employed relatively high polymer fluxes ($10 < Q_i/Q_S < 30$) and high injection velocities (10 %–40 % of the free stream speed) compared to the conditions of the other experiments shown in table 4.

6.3. *Mixing in the development region*

The development region was not measured in all test conditions in the present experiments, as its length was often less than the 2.09 m from the injector to the location of the second shear stress sensor. However, we can infer the development length through examination of both the $\%DR$ versus K plots and the c_M versus K plots. Both show the start of the precipitous drop in $\%DR$ and c_M with decreasing K (e.g. increasing distance from the injector location) over $1 \times 10^{-7} < K < 2 \times 10^{-7}$. Despite some remaining minor variation with U, the observation that the K-factor is somewhat successful at scaling the length of the development region X_D supports the notion that the phenomena leading to PDR in this region are coarsely determined by outer-flow TBL parameters. This is consistent with the development of the 50 % thickness of the concentration layer described by Petrie *et al.* (2003, 2005). They reported that the measured concentration layer thickness was typically much less than $0.1\delta_{99}$, in the development region, $1 \times 10^{-7} < K < 2 \times 10^{-7}$. For $K < 1 \times 10^{-7}$, the concentration thickness rapidly increases, with $\lambda/\delta_{99} > 0.5$ for $K < 10^{-8}$. The rate of polymer mixing is variable, but roughly corresponds to $K^{0.2}$ where the 0.2-exponent has some uncertainty. In addition, the injected polymer solutions have relaxation times of the order of 0.1 s while the integral fluctuation time scale of the TBL, δ_{99}/U, is of order 10^{-3} s near the injector. Hence, the injected high-concentration polymer solutions will not be easily deformed by the relatively high-frequency velocity fluctuations in the incoming TBL. Rather, the injected polymer will be strained by the mean near-wall shear flow.

6.4. *Mixing in the transitional and final regions*

The transitional region occupies $2 \times 10^{-7} > K > 4 \times 10^{-8}$ with the bounds varying slightly with U and M_w. The mixing rate is not constant over this region, but roughly scales as $K^{2.7}$ (compared to the exponent of 2.5 reported by Petrie *et al.* (2005), for WSR-N60K.) Again, it is helpful to compare using K versus $\%DR$ plots. Over this range of K, the $\%DR$ decreases from its peak to something of the order of 10%–20 %.

By the end of the transitional mixing region, the wall concentrations decrease from 100 w.p.p.m. to around 10 w.p.p.m., but significant turbulence modification is still possible with concentrations as low as a few w.p.p.m. and non-zero levels of drag reduction are still observed. The mixing rate decreases in the final region, where the polymer has been diluted to less than 10 w.p.p.m. and is largely mixed throughout the TBL, for $2 \times 10^{-8} K > 6 \times 10^{-8}$. The rate of concentration reduction scales with the growth of the TBL due to entrainment, with a growth rate of $\sim K^{6/7}$, the entrainment rate of a high-Reynolds-number TBL with little or no friction drag reduction. By $K \sim 10^{-9}$, the drag reduction is of the order of a few per cent and the concentration has typically fallen to less than 1 w.p.p.m..

6.5. *Filamentation of high-concentration polymer solutions*

The PLIF measurements of the near-wall concentration field often exhibited significant non-uniformity. Individual images reveal the near absence of polymer near the wall with high-concentration strands of polymer away from the wall. Vlachogiannis and Hanratty (2004) observed similar processes of polymer filamentation in their study of wall-injected polymer in a channel flow. They concluded that the presence of polymer filaments resulted in enhanced drag reduction, and

https://doi.org/10.1017/S0022112008004874 Published online by Cambridge University Press

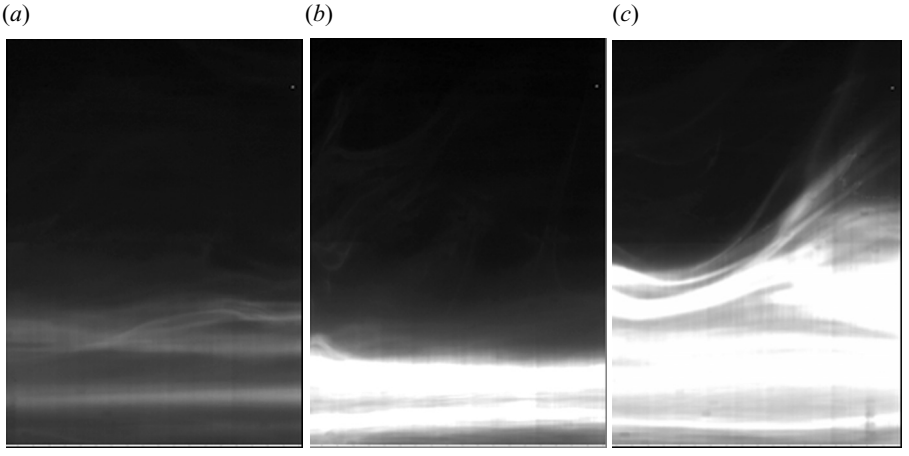


FIGURE 10. Three images of the near-wall polymer concentration fields taken in the filamented region in which $K > 2.4 \times 10^{-7}$ (WSR-301, $Q_i/Q_s = 10$, $C_i = 4000$ w.p.p.m., $U = 6.65\,\mathrm{m\,s^{-1}}$). Three types of images are common: (*a*) images with minimal polymer concentration (*b*) images that appear to have a thin sheet of polymer flowing along the model surface and (*c*) images with large amounts of filaments both along the model surface and lofted away from the surface. The flow is from left to right, and the dashed line denotes the location of the solid wall. The stretched field of view is 5 mm (streamwise) by 2.25 mm (wall normal).

this may be caused by the formation of polymer aggregates, as previously suggested by Cox, Dunlop & North (1974). As discussed above, it is likely that there is substantial aggregation in the injected polymer solutions. The high elasticity of the injected solutions leads them to be drawn from the injector, which introduces three-dimensional non-uniformity to the near-wall concentration field. Thus, polymer filamentation may cause there to be polymer-free regions near the injector, where little or no drag reduction is expected. This may play an important role in explaining the increase in $\%DR$ with downstream distance in the development region.

Examination of the PLIF images shows that for $K > 2.4 \times 10^{-7}$, the concentration field is very non-uniform, with large regions of nearly pure water and high polymer concentrations in elongated filaments. Figure 10 shows three sample images. As the polymer diffuses from the filaments into the surrounding solvent, the background concentration of the polymer increases. For the K values between 5×10^{-8} and 2.4×10^{-7}, the near-wall region consists of polymer filaments with a background of somewhat homogeneous polymer solution (see figure 11). In this region, the peak drag reduction has occurred and mixing into the log-layer has been commenced. Finally, with $K < 5 \times 10^{-8}$, the filaments have been mixed into the flow and the concentration fields are nearly uniform (images not provided).

7. Comparison of observed and expected levels of drag reduction with varying M_w

With the data presented above, we can construct empirical drag reduction curves based on the drag-reducing characteristics of each polymer. The polymer parameters used are the intrinsic drag reduction $[\%DR] = \lim_{C\to 0}(\%DR/c_M)$, a quantity relating to the drag-reducing efficiency of a given polymer and the intrinsic concentration, $[C] = \%DR_{MAX}/[\%DR]$. These quantities were first introduced for pipe-flows by Virk *et al.* (1967). The polymer-specific quantities $[\%DR]$ and $[C]$ were determined from a

https://doi.org/10.1017/S0022112008004874 Published online by Cambridge University Press

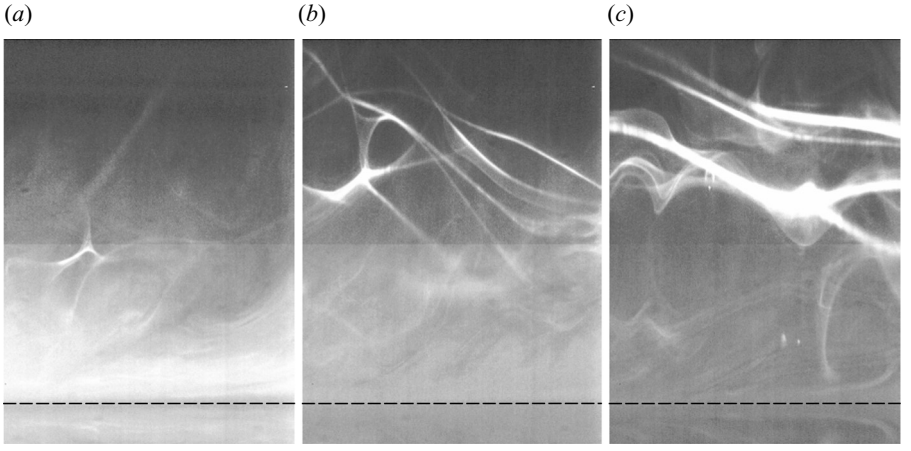


FIGURE 11. Three images of the near-wall polymer concentration fields taken in the transition region between highly filamented and uniform regions ($5.3 \times 10^{-8} < K < 2.4 \times 10^{-7}$; WSR-301, $Q_i/Q_s = 2$, $C_i = 4000$ w.p.p.m., $U = 6.65\,\mathrm{m\,s^{-1}}$). This flow regime is characterized by periodic filaments in a somewhat uniform background polymer concentration. The images selected show various examples of background polymer concentration with lofted polymer filaments. The flow is from left to right, and the dashed line denotes the location of the solid wall. The stretched field of view is 5 mm (streamwise) by 2.25 mm (wall normal).

	U (m s^{-1})	$\%DR$ (w.p.p.m.$^{-1}$)	C (w.p.p.m.)
WSR-N60K	6.65	6	7
	13.2	6	8
	19.9	4	12
	All	**5**	**10**
WSR-301	6.65	32	2
	13.2	25	2
	19.9	17	3
	All	**26**	**2**
WSR-308	6.65	73	1
	13.2	27	3
	19.9	14	5
	All	**32**	**2**

TABLE 5. The intrinsic drag reduction, $\%DR$, and intrinsic concentration, C, for the near-wall polymer solutions. The values for each speed and for all speeds combined are presented. The fitted curves are shown in figure 12.

best fit of the experimental data to a relationship of the form

$$\frac{\%DR}{c_M} = \frac{[\%DR]}{1 + c_M/[C]}, \tag{7.1}$$

also introduced by Virk *et al.* (1967). Figure 12 presents $\%DR/c_M$ as a function of c_M for the three M_w polymers demonstrating a reasonable collapse of the data. Table 5 presents the intrinsic parameters of each of the three polymers as a function of speed as well as the average values when fitted to the data from all test speeds. Despite the mild scatter in the data, some of the general trends are apparent. As expected,

https://doi.org/10.1017/S0022112008004874 Published online by Cambridge University Press

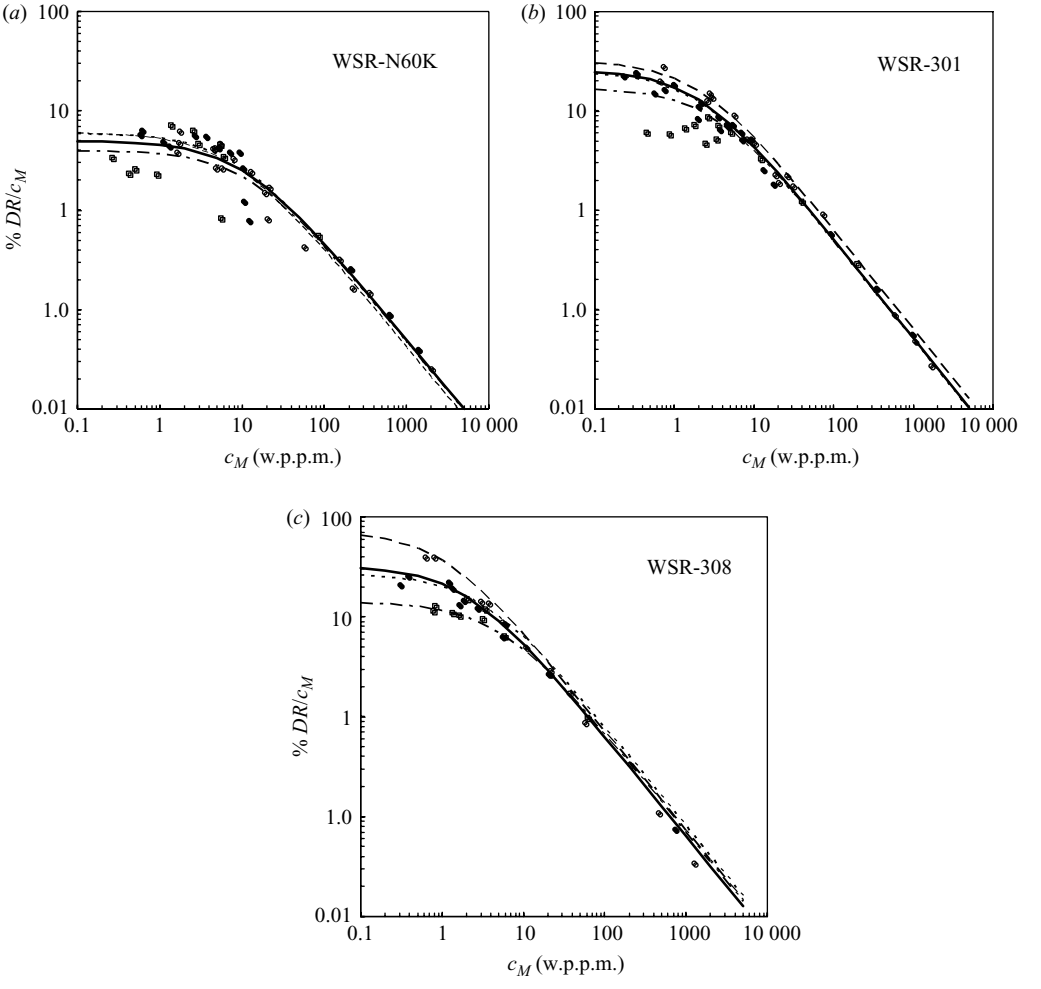


FIGURE 12. The $\%\mathrm{DR}/\mathrm{c}_M$ versus c_M for the three M_w examined: $U = 6.65$ (○), 13.2 (●) and 19.9 (□) $\mathrm{m\,s^{-1}}$. Curves fitted to (7.1) are plotted for each speed (dashed lines) and for all speeds together (solid line). Values of intrinsic drag reduction and intrinsic concentration derived from the fitted curves are provided in table 5.

the drag-reducing efficiency increases with polymer M_w with $[\%DR]$ for WSR-308 on average ∼1.2 times greater than WSR-301, and WSR-301 on average ∼5 times greater than WSR-N60K. Also, $[\%DR]$ was observed to decrease with increasing free stream speed and the effects of free stream speed are more pronounced with increasing M_w. Pipe-flow studies have shown that for a given polymer type and concentration, $\%DR$ will increase with increasing speed, i.e. flow-rate, in the absence of degradation. Correspondingly, the $[\%DR]$ would be expected to increase with speed as the Weissenberg number increases (Virk *et al.* 1967), whereas the converse is true for the present data. The fact that a decrease in $[\%DR]$ with increasing speed is observed in the present data indicates the higher M_w polymers are subject to flow-induced degradation.

Vanapalli *et al.* (2005) have shown that high-molecular-weight PEO solutions like WSR-308 undergo significant degradation in turbulent shear flows when shear rates

https://doi.org/10.1017/S0022112008004874 Published online by Cambridge University Press

exceed those given by (4.7). Continued exposure to shear rates that will sufficiently stretch the molecules to cause scission results in continual reduction in M_w, until M_w is reduced to the point that the molecules are scission resistant at the shear rates of the flow. The flow conditions of the present study generate sufficiently high shear rates so that the higher M_w polymer molecules, experiencing the greatest strain, would be expected to continually degrade, effectively reducing the mean M_w. Vanapalli *et al.* (2006) analysed the scaling of polymer scission in wall-bounded turbulent shear flow and found that the bulk of the polymer degradation takes place in the log layer of the TBL, since this is where the appropriate combination of volume flux and shear rate is highest. While no samples were drawn from the near-wall flow and no direct measurements of M_w were made from polymer exposed to the flow, data presented here suggest that substantial degradation is occurring when the higher M_w polymers are used. The streamwise extent of the present test model appears to be sufficient to reveal the presence of degradation, indicating that degradation time scales are of the order of 1 s or less.

8. Summary and conclusions

A unique large-scale high-Reynolds-number experimental investigation into the TBL skin-friction drag reduction caused by the injection of polymer solutions has been conducted in the world's largest low-turbulence water tunnel. These experiments provide new laboratory results for TBL skin-friction drag reduction at Reynolds numbers and downstream distances that are within an order of magnitude of those typical of full-scale ships, and allow a direct assessment of the skin-friction drag-reduction performance of different molecular weights of PEO injected at three flow-rates and three concentrations. Measurements of skin friction and near-wall polymer concentration were made from less than 1 m to more than 9 m downstream of the injector at free stream flow speeds from 6.65 to 19.9 m s^{-1}. The combination of co-located skin-friction measurements and images of the near-wall polymer concentration field provides new insights into polymer-induced drag reduction and diffusion in a TBL. Scatter in the experimental data is comparable to similar prior smaller scale investigations.

Measurements suggest that three flow regimes exist in polymer-induced skin-friction drag reduced TBL flows: a near-injector development region where the polymer solution is located primarily near the wall, filaments are commonly observed and drag-reduction increases with downstream distance; a transitional region where the polymer solution is mixed from the wall through the rest of the boundary layer, filaments are less pronounced and drag reduction drops precipitously; and a final region where significant levels of drag reduction are lost, drag reduction decreases at a slower rate and dilution of the polymer occurs at a rate set by the boundary layer turbulence. Interestingly, the closest approach to the MDR asymptote (Virk *et al.* 1970) is observed as the flow moves from the first to the second regime.

The development region near injection is characterized by levels of drag reduction that increase with downstream distance. PLIF images of polymer concentration show that the injected polymer is neither confined to a well-defined near-wall layer nor homogeneously distributed, but instead was drawn from the wall-layer in filaments by its interaction with boundary layer turbulence, leading to nearly binary distributions of polymer. The increase in drag reduction with downstream distance can be explained by the following phenomena: (*a*) regions of high concentration and high drag reduction may exist, but off-set by regions of essentially zero drag reduction, resulting in low

https://doi.org/10.1017/S0022112008004874 Published online by Cambridge University Press

drag reduction on the integral sense, (*b*) mixing through the buffer region is needed before the significant turbulence modification takes place and (*c*) a finite amount of time is required for the polymer molecules to be stretched and activated by the flow. The development region ends with the flow's nearest approach to MDR at K values of approximately 1×10^{-7} or 2×10^{-7}, and coincidentally, drag reduction was not observed to persist near MDR for any significant distance. The length of the development region was observed to increase with increasing M_w, injection concentration and injection rate and decreasing free stream speed, and is roughly proportional to the quantity $Q_i C/U$ for a given M_w. The development length was not observed at the highest flow speed but extended as far as 6 m from the point of injection at the lowest speed.

The transitional region occurs downstream of the flow's nearest approach to MDR and is characterized by a precipitous drop in drag reduction and near-wall polymer concentration with downstream distance. Polymer filaments may still persist into the transitional region, yet the concentration field is less binary as the polymer mixes from the wall into the inter-filament fluid. Here, the traditional K-factor scaling provides an adequate collapse of the drag reduction and concentration data, and the near-wall concentration in this region is observed to decrease with distance at a rate proportional to $K^{2.7}$. While the general slope of decreasing drag reduction with decreasing K in this region agrees with prior studies, distinct speed dependence is observed for the higher M_w polymers, not reported in smaller scale and lower speed experiments. For equivalent values of K in the transitional region, higher levels of drag reduction were achieved with decreasing free stream speed. It is postulated that the observed speed dependence may be caused by flow-induced chain-scission of the molecules, as the shear rates of the present study are well beyond the scission degradation values for PEO in pipe flow (Vanapalli *et al.* 2005). The combination of high flow speeds and model length of the present study may be necessary to observe the impact of such polymer degradation.

The final region is characterized by low levels of drag reduction and drastically reduced near-wall concentration, as the polymer is mixed throughout the boundary layer. The rate of mixing and dilution in this region is proportional to the rate set by the entrainment of free stream fluid. In this region, the traditional K-scaling of drag reduction is adequate, yet the drag reduction is sufficiently low to be of little interest for practical applications.

A relationship between near-wall polymer concentration and drag reduction in a TBL has been generated based on the intrinsic properties of a given polymer solution in the form of a empirical drag reduction curve. In contrast to pipe flows, the present data show that the intrinsic drag reduction, i.e. drag-reducing efficiency, decreases with increasing free stream speed, and the decrease with speed is more pronounced with increasing M_w. The decrease in efficiency with speed indicates that the higher M_w polymer molecules are subject to chain-scission and the extent of degradation increases with M_w.

The authors would like to acknowledge significant contributions to this work from our colleagues at The University of Michigan, the Naval Surface Warfare Center and the overall DARPA Friction Drag Reduction Program. We would like to acknowledge the helpful discussions we had with many members of the DARPA Friction Drag Reduction Program, with special thanks to Mr Duncan Brown and Dr Howard Petrie. This work was supported by DARPA under contract number HR0011–04-1–0001, Dr Thomas Beutner, Program Manager. The content of this document does not

https://doi.org/10.1017/S0022112008004874 Published online by Cambridge University Press

necessarily reflect the position or policy of the United States Government, and no official endorsement should be inferred.

REFERENCES

Almeida, T. G., Walker, D. T., Leighton, R. I., Alajbegovic, A., Pankajakshan, R., Taylor, L. K., Whitfield, D. L. & Ceccio, S. L. 2006 A Reynolds-averaged model for the prediction of friction drag reduction by polymer additives. In *Proceedings of the 26th Symposium on Naval Hydrodynamics*, Rome.

Bailey, F. E. & Callard, R. W. 1959 Some properties of poly(ethylene oxide) in aqueous solutions. *J. Appl. Polym. Sci.* **1** (1), 56–62.

Batchelor, G. K. 1957 Diffusion in free turbulent shear flows. *J. Fluid Mech.* **3** (1), 67–80.

Beris, A. & Dimitropoulos, C. 1999 Pseudospecrtral simulation of turbulent viscoelastic channel flow. *Comput. Methods Appl. Mech. Eng.* **180**, 365–392.

Brungart, T. A., Petrie, H. L., Harbison, W. L. & Merkle, C. L. 1991 A fluorescence technique for measurement of slot injected fluid concentration profiles in a turbulent boundary layer. *Exp. Fluids* **11**, 9–16.

Cox, L. R., Dunlop, E. H. & North A. M. 1974 Role of molecular aggregates in liquid drag reduction by polymers. *Nature* **249** (5454), 243–245.

Dealy, J. M. & Larson, R. G. 2006 *Structure and Rheology of Molten Polymers*. Hanser Gardener Publications.

Dubief, Y., White, C. M., Terrapon, V. E., Shaqfeh, E. S. G., Moin, P. & Lele, S. K. 2004 On the coherent drag-reducing and turbulence-enhancing behaviour of polymers in wall flows. *J. Fluid Mech.* **514**, 271–280.

Dunlop, E. H. & Cox, L. R. 1977 Influence of molecular aggregates on drag reduction. *Phys. Fluids* **20**, S203–S213.

Etter R. J., Cutbirth, J. M., Ceccio, S. L., Dowling, D. R. & Perlin, M. 2005 High Reynolds number experimentation in the U. S. Navy's William B. Morgan Large Cavitation Channel. *Measur. Sci. Technol.* **16** (9), 1701–1709.

Faraone, A., Magazu, S., Maisano, G., Migliardo, P., Tettamanti, E. & Villari, V. 1999 The puzzle of poly(ethylene oxide) aggregation in water: Experimental findings. *J. Chem. Phys.* **110**, 1801–1806.

Fontaine, A. A., Petrie, H. L. & Brungart, T. A. 1992 Velocity profile statistics in a turbulent boundary layer with slot-injected polymer. *J. Fluid Mech.* **238,** 435–466.

Fruman, D. H. & Tulin, M. P. 1976 Diffusion of a tangential drag-reducing polymer injection on a flat plate at high Reynolds number. *J. Ship Res.* **20** (3), 171–180.

Ho, D. L., Hammouda, B. & Kline, S. R. 2003 Clustering of poly(ethylene oxide) in water revisited. *J. Polym. Sci.* B **41**, 135–38.

Horn, A. F. & Merrill, E. W. 1984 Midpoint scission of macromolecules in dilute solution in turbulent flow. *Nature* **312**, 140–141.

Housiadas, K. D. & Beris, A. N. 2003 Polymer induced drag reduction: effects of the variations in elasticity and inertia in turbulent viscoelastic channel flow. *Phys. Fluids* **15** (8), 2369–2384.

Jimenez, J. & Pinelli, A.1999 The autonomous cycle of near-wall turbulence. *J. Fluid Mech.* **389**, 335–359.

Kalashnikov, V. N. 1994 Shear-rate dependent viscosity of dilute polymer solutions *J. Rheol.* **38**, 1385–1403.

Kalashnikov, V. N. 1998 Dynamical similarity and dimensionless relations for turbulent drag reduction by polymer additives. *J. Non-Newton. Fluid Mech.* **75**, 209–230.

Lotto, B. & El Riedy, O. K. 1981 Effects of sampling rate on concentration measurements in non-homogeneous dilute polymer solution flow. *J. Rheol.* **25** (6), 583–590.

Patel, V. C. 1965 Calibration of the Preston tube and limitations on its use in pressure gradients. *J. Fluid Mech.* **23**, 185–208.

Petrie, H. L., Brungart, T. A. & Fontaine, A. A. 1996 Drag reduction on a flat plate at high Reynolds number with slot-injected polymer solutions. In *Proceedings of the ASME Fluids Engineering Division* **237**, 3–9.

https://doi.org/10.1017/S0022112008004874 Published online by Cambridge University Press

Petrie, H. L., Deutsch, S., Brungart, T. A. & Fontaine, A. A. 2003 Polymer drag reduction with surface roughness in flat-plate turbulent boundary layer flow. *Exp. Fluids* **35**, 8–23.

Petrie, H. L. & Fontaine, A. A. 1996 Comparison of turbulent boundary layer modifications with slot-injected and homogeneous drag-reducing polymer solutions. In *Proceedings of the ASME Fluids Engineering Division* **237**, 205–210.

Petrie, H., Fontaine, A., Money, M. & Deutsch, S. 2005 Experimental study of slot in injected polymer drag reduction. In *Proceedings of the 2nd International Symposium on Seawater Drag Reduction*. Busan 605–620.

Polverari, M. & van de Ven, T. G. M. 1996 Dilute aqueous poly(ethylene oxide) solutions: clusters and single molecules in thermodynamic equilibrium. *J. Phys. Chem.* **100**, 13687–95.

Poreh, M. & Cermak, J. E. 1964 Study of diffusion from a line source in a turbulent boundary layer. *Intl J. Heat Mass Transfer* **7** (10), 1083–1095.

Poreh, M. & Hsu, K. S. 1972 Diffusion of drag reducing polymers in a turbulent boundary layer. *J. Hydronaut*. **6** (1), 27–33.

Ptasisnski, P. K., Boersma, B. J., Nieuwstadt, F. T., M., Hulsen, M. A., van den Brule, A. & Hunt, J. C. R. 2003 Turbulent channel flow near maximum drag reduction: simulations, experiments and mechanisms. *J. Fluid Mech.* **490**, 251–291.

Sanders, W. C., Winkel, E. S., Dowling, D. R., Perlin, M. & Ceccio, S. L. 2006 Bubble friction drag reduction in a high-Reynolds number flat-plate turbulent boundary layer. *J. Fluid Mech.* **552**, 2006, 353–380.

Schultz-Grunow, F. 1941 New frictional resistance law for smooth plates. *NACA Tech. Memorandum* **17** (8), 1–24.

Sellin, R. H. J. 1982 The effect of drag-reducing additives on fluid flows and their industrial applications part 2: present applications and future proposals. *J. Hydraul. Res.* **20** (1), 29–69.

Sommer, S. T. & Petrie, H. L. 1992 Diffusion of slot injected drag-reducing polymer solution in a LEBU modified turbulent boundary layer. *Exp. Fluids* **12**, 181–188.

Tirtaatmadja, V., McKinley, G. H. & Cooper-White. J. J. 2006 Drop formation and breakup of low viscosity elastic fluids: effects of molecular weight and concentration. *Phys. Fluids* **18**, 043101.

Vanapalli, S. A. 2007 Polymer chain scission in extensional and turbulent flows and implications for friction drag technologies. Ph.D. dissertation, University of Michigan.

Vanapalli, S. A., Ceccio, S. L. & Solomon, M. J. 2006 Universal scaling for polymer chain scission in turbulence. In *Proceedings of the National Academy of Science* **103** (45), 16660–16665.

Vanapalli, S. A., Islam, M. T. & Solomon, M. J. 2005 Scission-induced bounds on maximum polymer drag reduction in turbulent flow. *Phys. Fluids* **17**,1–11.

Vdovin, A. V. & Smol'yakov, A. V. 1978 Diffusion of polymer solutions in a turbulent boundary layer. *J. Appl. Mech. Tech. Phys.* **19** (2), 66–73.

Vdovin, A. V. & Smol'yakov, A. V. 1981 Turbulent diffusion of polymers in a boundary layer. *J. Appl. Mech. Tech. Phys.* **22** (4), 98–104.

Virk, P. S. 1975 Drag reduction fundamentals. *J. Am. Inst. Chem. Eng.* **21** (4), 625–656.

Virk, P. S., Merrill, E. W., Mickley, H. S., Smith, K. A. & Mollo-Christensen, E. L. 1967 The Toms phenomenon: turbulent pipe flow of dilute polymer solutions. *J. Fluid Mech.* **30** (2), 305–328.

Virk, P. S., Mickley, H. S. & Smith, K. A. 1970 The ultimate asymptote and mean flow structure in Toms' phenomenon. *Trans. ASME: J. Appl. Mech.* **37** (2), 488–493.

Vlachogiannis, M. & Hanratty, T. J. 2004 Influence of wavy structured surfaces and large scale polymer structures on drag reduction. *Exp. Fluids* **36**, 685–700.

Vlassopoulous, D. & Schowalter, W. R. 1994 Steady viscometric properties and characterization of dilute drag-reducing polymer solutions *J. Rheol.* **38**, 1427–1446.

Walker, D. T., Tiederman, W. G. & Luchik, T. S. 1986 Optimization of the injection process for drag-reducing additives. *Exp. Fluids* **4**, 114–120.

Warholic, M. D., Massah, H. & Hanratty, T. J. 1999 Influence of drag-reducing polymers on turbulence, effects of Reynolds number, concentration, and mixing. *Exp. Fluids* **27**, 461–472.

White, F. M. 2005 *Viscous Fluid Flow* (3rd ed.). McGraw-Hill.

https://doi.org/10.1017/S0022112008004874 Published online by Cambridge University Press

White, C. M., Somandepalli, V. S. R. & Mungal, M. G. 2004 The turbulence structure of drag reduced boundary layer flow. *Exp. Fluids* **36**, 62–69.

Winkel, E. S., Oweis, G., Vanapalli, S. A., Dowling, D. R., Perlin, M., Solomon, M. J. & Ceccio, S. L. 2006 Friction drag reduction at high Reynolds numbers with wall injected polymer solutions. In *Proceedings of the 26th Symposium on Naval Hydrodynamics*, Rome.

Wu, J. & Tulin, M. P. 1972 Drag reduction by ejecting additive solutions into pure-water boundary layer. *Trans. ASME: J. Basic Engng* **94**, 749–756.

https://doi.org/10.1017/S0022112008004874 Published online by Cambridge University Press